Oxalyl Chloride—A Clean Source of Chlorine Atoms for Kinetic Studies

Alexey V. Baklanov[†] and Lev N. Krasnoperov*

Department of Chemical Engineering, Chemistry and Environmental Science, New Jersey Institute of Technology, University Heights, Newark, New Jersey 07102

Received: May 26, 2000; In Final Form: October 18, 2000

Oxalyl chloride, $(COCl)_2$, has been characterized as a photolytic source of chlorine atoms for kinetic studies. UV absorption spectrum of oxalyl chloride, as well as the photodissociation yield of chlorine atoms resulting from the photodissociation of oxalyl chloride at 193 nm (ArF excimer laser) in helium as a bath gas at $p_{He} = 1$, 10, and 100 bar, were measured using laser pulsed photolysis—UV−vis transient absorption spectroscopy. The photodissociation yield of chlorine atoms was determined from the measurements of photodepletion of oxalyl chloride via its absorption at 210.0 nm as well as via 270−390 nm UV absorption build-up caused by molecular chlorine formed in the recombination of chlorine atoms. The photodissosiation yield of chlorine atoms (the number of Cl atoms appeared per one dissociated oxalyl chloride molecule) is independent of helium pressure over the pressure range 1−100 bar. The photodissociation yields of chlorine atoms at 298 K were measured as 2.01 ± 0.08 and 1.97 ± 0.12 at $p_{He} = 10$ bar and $p_{He} = 100$ bar, respectively. The overall photodissociation of oxalyl chloride at 193 nm is described by the following stoichiometric equation: $(COCl)_2 + h\nu(193\ nm) \rightarrow 2\ CO + 2\ Cl$. Due to the absence of any additional reactive species in the final photodissociation products, its relatively large absorption cross-sections in the UV and low reactivity toward free radicals, oxalyl chloride is suggested as a convenient and "clean" photolytic source of Cl atoms for kinetic studies.

Introduction

Direct kinetic studies of elementary reactions of atoms and free radicals using pulsed photolysis technique require convenient and clean photolytic sources of these transient species. Ideally, a photolytic precursor should have reasonably large absorption cross-section, should produce only the transient species of interest, and should be relatively inert toward reactions with atoms and free radicals participating in the subsequent secondary reactions. Chlorine atoms, due to their high reactivity and relative simplicity of photo generation were often used for the secondary radical production via H-atom abstraction from a proper secondary photolytic precursor. This approach was particularly fruitful for generation of silyl radicals, SiH_3,[1] where no good direct photolytic source has been found.[2] Several molecules, such as S_2Cl_2, CCl_4, NOCl, C_2Cl_6, $COCl_2$, Cl_2, have been reported as the photolytic sources of chlorine atoms.[2] However, none of them can be considered completely satisfactory, due to either production of other reactive intermediates, high reactivity toward chlorine atoms and/or silyl radicals, or high toxicity. In this work, oxalyl chloride is suggested as a clean source of chlorine atoms.

In recent years, there have been several studies of photochemistry of oxalyl chloride in the UV. Schroeder et al.[3] studied the UV light induced photoisomerization of oxalyl chloride in Ar and Xe matrixes using Fourier Transform IR spectroscopy. In a xenon matrix, the formation of CO and phosgene ($COCl_2$) was observed in addition to the photoisomerization product. Ahmed et al.[4] studied photodissociation of oxalyl chloride, $(COCl)_2$, at 235 nm in a molecular beam using the photofragment imaging technique. Both Cl atoms and CO were found as photodissociation products. The same products were observed by Hemmi and Suits[5] in their study of the photodissociation dynamics of oxalyl chloride at 193 nm using the photofragment translational spectroscopy.

In this work, the photodissociation of oxalyl chloride was studied at 193 nm in the gas phase in excess of helium at $p_{He} = 1$, 10, and 100 bar using pulsed excimer laser (ArF, 193 nm) photolysis combined with transient UV-absorption spectroscopy. The main objective of the study was the determination of the photodissociation yield of Cl atoms. The photodepletion of the oxalyl chloride was monitored by UV absorption measurements at 210.0 nm. UV-absorption in the region of 270−390 nm was used to monitor molecular chlorine, Cl_2, produced in the reaction of Cl atoms recombination. In this work, UV absorption cross-sections of oxalyl chloride combined with the accurately known absorption cross-sections of molecular chlorine allowed to determine the photodissociation yield of chlorine atoms—the number of chlorine atoms produced per one dissociated molecule of oxalyl chloride.

Experimental Section

The experimental approach is described in detail elsewhere.[6] The experimental setup was a combination of a pulsed excimer laser photolysis, transient UV−vis spectroscopy with a high-pressure flow system. A reactant mixture that contained oxalyl chloride $(COCl)_2$ and a buffer gas (He) in great excess (10^3−10^5 times) was flowing through a high-pressure absorption cell. The cell (internal diameter 7.2 mm, internal length 10.4 cm, volume 4.2 cm^3) is equipped with two thick fused silica windows and is designed to withstand pressures up to at least

* To whom correspondence should be addressed: Lev N. Krasnoperov, Department of Chemical Engineering, Chemistry and Environmental Science, New Jersey Institute of Technology, University Heights, Newark, New Jersey 07102. E-mail: krasnoperov@adm.njit.edu.

[†] On leave from the Institute of Chemical Kinetics and Combustion, Novosibirsk 630090, Russia.

10.1021/jp0019456 CCC: $20.00
Published on Web 12/02/2000

150 bar. Oxalyl chloride concentrations were in the range (1.2−2.4) × 10^{16} molecule cm^{-3}. The typical energy flux of the ArF excimer laser light (λ = 193 nm) was ca. 20 mJ cm^{-2}. The experiments were performed at three buffer gas pressures: 1, 10, and 100 bar. Helium was used as a buffer gas. All experiments were done at ambient temperature 300 ± 3 K. The experiments were performed under the conditions of complete replacement of the reaction mixture between the laser pulses using proper gas flows (3−60 standard cubic centimeter per second) and repetition rates (such as 0.5 Hz at 1 bar and 0.1 Hz at 100 bar).

An unfocused light from an ArF excimer laser (Lumonics TE−861T-3) was formed into a beam by two iris diaphragms and reflected by a 45° (>98% at 193 nm, Newport) dielectric mirror and directed along the cell axis so that it filled all of the cross-section of the cell. When reflected by the dielectric mirror, the laser beam was merged with the monitoring beam that was formed by a fused silica lens (f = 10 cm). After passing the cell, the laser beam was separated from the monitoring light using the second 45° dielectric mirror for 193 nm.

Hollow cathode lamps (HCL) as well as a low-power Xe arc lamp (75 W) were used as sources of the monitoring light. To improve the monitoring light intensity, a three-electrode hollow cathode lamp (Superlamp, Photron), with square pulses at 4 Amp current and 3 ms duration, was used with current boosting.

The light from a hollow cathode or Xe arc lamp was focused into the cell and then onto the entrance slit of a grating monochromator (Jarrell-Ash, Model 82-518, 0.5 m) using two fused silica lenses with focal lengths of 10 cm. The residual light from the excimer laser pulse was removed using a spatial filter (1 mm diameter wire placed perpendicular to the slit in the focal spot of the second lens) and by a liquid filter (4.3 × 10^{-2} M solution NaCl in water, 1 cm). The liquid filter provided depression of 193 nm light 10^{12} times while attenuating the monitoring light (210.0 nm) only by about 20%. A photomultiplier tube (Hamamatsu R106) mounted on the exit slit operated on the reduced number of dynodes (6) with the voltage divider current of 2.7 mA, which ensured good linearity and lower noise at high photon fluxes. The PMT signal was preamplified (EMI preamplifier), then digitized and stored using a digital storage oscilloscope (LeCroy 9310A, Dual channel, 400 MHz, 100 Msamples/s, 50 Kpts/ch). The time resolution was determined by the preamplifier settings. Time constants of 0.3 μs or 3 μs were used in the measurements of oxalyl chloride depletion. Much longer time constant (100 μs, using an additional three-stage RC filter) was used to record the absorption build-up due to the formation of molecular chlorine. In addition, the PMT signal was biased to zero using an external adjustable bias voltage supply. The bias voltage was adjusted to compensate the PMT signal due to the monitoring light in the absence of the laser pulse. As a result, the most sensitive scales of the oscilloscope for the data acquisition were used and the accuracy of the measurements of small changes of the probing light intensity caused by the formation of molecular chlorine was significantly improved. After the signal accumulation (about 300 pulses), the traces were transferred to a PC for processing.

A light shutter (Oriel Model 76993) was installed between the laser and the cell. Every even laser pulse was blocked. A synchronized switch (Pasternack Electronics, PE7100) was used to connect the two input channels of the oscilloscope to the preamplifier output to accumulate separately the light intensity profile with and without the laser pulse entering the reactor. This procedure was used to account for a small (0.5% in 1 ms) variation of the monitoring light intensity during a pulse. The two traces then were used to calculate the temporal profile of the monitoring light absorption.

TABLE 1: Absorption Cross-Sections of Oxalyl Chloride at Different Wavelengths Measured in This Work

wavelength/nm	absorption cross-section[a]/ 10^{-20} cm^2 $molecule^{-1}$
193.3	383 ± 10
210.0	246 ± 3
217.9	118
248	27
270	15
300	8.0
308	7.1
330	6.3 ± 0.3
334.2	5.8
360	1.6
390	0.15

[a] The error of the data obtained at the wavelengths other than 193.3, 210.0, and 330 nm is estimated to be better or about 10% of the presented value and somewhat worse (15−20%) for the last two wavelengths.

The high-pressure flow system consists of high-pressure mass flow controllers, a high-pressure flow cell, an upstream (back) pressure regulator, high-pressure test gauges, and cylinders with helium, the precursor, and the reactant mixtures. Brooks high-pressure mass flow controllers (5850 TR series) and Brooks electronic upstream pressure regulator (model 5866) were used. The flow controllers were periodically calibrated using the soap film method. The flow reactor pressure was measured using test pressure gauges (Matheson Model 63-5633M, up to 250 bar, Model 63-5622M, up to 14 bar, accuracy 0.25%) and by the internal calibrated pressure sensor of the electronic upstream pressure regulator.

Oxalyl chloride (98%, Aldrich Chem. Co.) was degassed by a freeze−pump−thaw procedure from liquid nitrogen. Then it was purified from a possible molecular chlorine impurity by pumping the vapor of an oxalyl chloride sample at a temperature slightly above its melting point (−8 − −10 °C). After the oxalyl chloride degassing and purification, mixtures $(COCl)_2$/He of known compositions were prepared. When high-pressure (150 bar) mixtures were used, proper corrections for the nonideal behavior were introduced based on the tabulated compression factors.[7]

Helium from Matheson (UHP grade, 99.999%) was passed through an oxygen trap (R&D Separations, Model OT3-2) to ensure molecular oxygen content less than 0.02 ppm.

The absorption cross-sections of oxalyl chloride were measured at several fixed wavelengths: 193 nm (ArF laser as a light source), 210.0 nm (Zn hollow cathode lamp), 217.9, and 249.2 nm (Cu hollow cathode lamp)) and within the 270−390 nm region (Xe arc lamp). The photodepletion of oxalyl chloride absorption resulted from the ArF laser pulse was measured at 210.0 nm (Zn HCL). The absorption of molecular chlorine arising in the recombination of Cl atoms was probed in the 270−390 nm range (Xe arc lamp), with most of the measurements performed at 330 nm. Portions of the optical path outside the cell between the cell windows and the merging dielectric mirrors were purged by nitrogen. This was done to avoid interference from the absorption of the monitoring light by ozone which is formed after photodissociation of molecular oxygen by the ArF laser radiation.

Results

UV absorption cross sections of oxalyl chloride measured at several wavelength from 193 to 390 nm are listed in Table 1

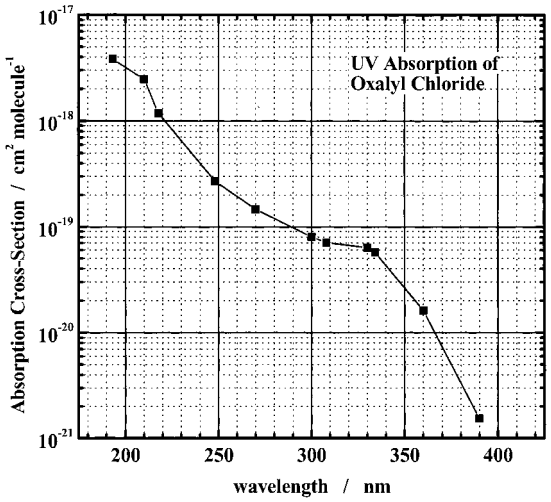

Figure 1. The absorption spectrum of gaseous oxalyl chloride at 297 K in helium (1 bar). Experimental points are shown by filled squares. The points are connected by straight lines.

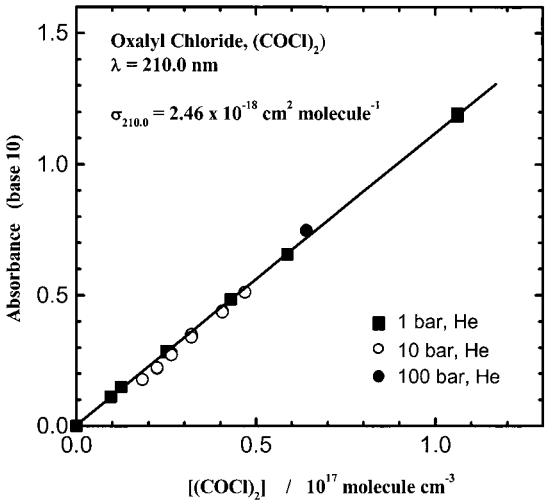

Figure 2. The absorbance (optical density, base 10) of gaseous oxalyl chloride vs. its concentration at wavelength 210.0 nm (hollow cathode Zn lamp). Different symbols correspond to different helium pressures: filled squares − 1 bar, open circles − 10 bar, and filled circles − 101 bar. The absorption cross-section $\sigma_{210.0}$ was obtained taking into account all points.

and plotted in Figure 1. The absorption cross-section at 210 nm was measured at several buffer gas pressures. No pressure dependence of the absorption was found within the experimental error (Figure 2). Fitting of the combined data yielded the absorption cross-section $\sigma_{210}((COCl)_2) = (2.46 \pm 0.03) \times 10^{-18}$ cm^2 molecule^{-1}. This value was used to calculate the concentration of oxalyl chloride photodissociated after a laser pulse. Additional checks on the pressure dependence were performed at the laser wavelength, 193.3 nm, as well as at 330 nm. No change (within 10%) in the absorption cross-section at these wavelengths was found when the pressure of helium changed from 1 to 101 bar.

A temporal profile of the transient absorption at 210.0 nm is shown in Figure 3. The changes of the oxalyl chloride absorption ($\ln(I/I_0)_{OxCl,210}$) were determined from the traces similar to one shown in this figure. In addition to the precursor photodepletion, the build-up of the absorption within the spectral region, which corresponds to the absorption peak of molecular chlorine, was measured. A typical temporal profile of molecular chlorine absorption is shown in Figure 4. The build-up of the absorption in this spectral range is due to the formation of molecular

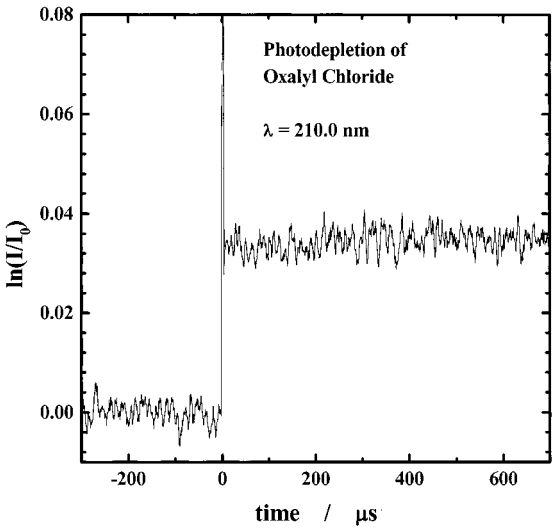

Figure 3. The photodepletion of oxalyl chloride by ArF laser radiation measured via UV absorption at 210.0 nm. The short spike is due to the scattered laser and the laser discharge light. The experimental conditions are $[(COCl)_2] = 2.4 \times 10^{16}$ molecule cm^{-3}; $p_{He} = 1$ bar; monitoring with a Zn hollow cathode lamp, wavelength 210.0 nm. The intensities I and I_0 correspond to the monitoring light intensity with and without ArF laser pulse entering the reactor, respectively.

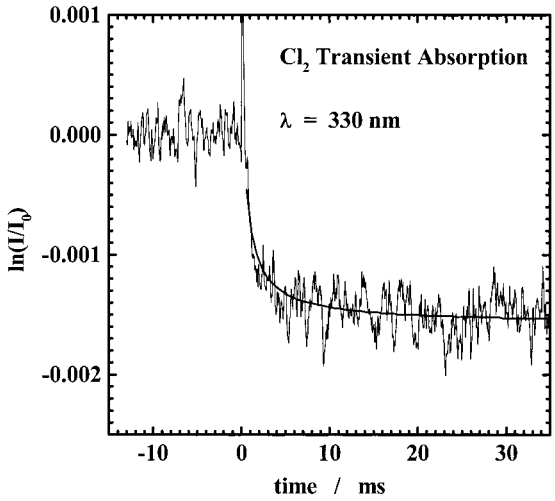

Figure 4. Sample temporal profile of the absorption at 330 nm (maximum absorption of molecular chlorine). The experimental conditions as in Figure 3.

chlorine which is produced in the reaction of chlorine atoms recombination

$$Cl + Cl\ (+\ He) \rightarrow Cl_2\ (+\ He) \qquad (1)$$

To increase the signal amplitude and to improve the accuracy of the measurements, we performed the experiments under the conditions of strong absorption (up to ca. 60%) of the laser light. In this case, the absorbance temporal profiles of are described by eq 2 (see Appendix). In this equation, Abs is the absorbance (base e, $\mathrm{Abs}(t) = -\ln(I/I_0)$) at the wavelength of the probing light. The experimental profiles were fitted by eq 2, the resulting best fit curve is illustrated in Figure 4.

$$\mathrm{Abs}(t) = A - C - \frac{B}{(t - t_0)} \ln\left\{\frac{\left[1 + \frac{A(t - t_0)}{B(1 - G)}\right]}{\left[1 + \frac{AG(t - t_0)}{B(1 - G)}\right]}\right\} \qquad (2)$$

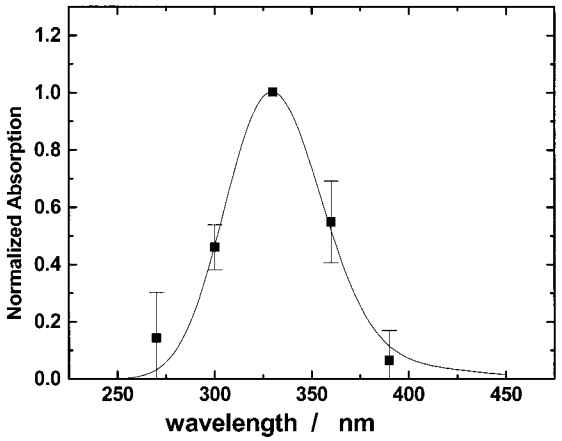

Figure 5. The correlation of the amplitude of the transient absorption in the range 270−390 nm with the absorption spectrum of molecular chlorine. Photodissociation of oxalyl chloride by ArF laser radiation pulse, $[(COCl)_2] = 2.4 \times 10^{16}$ molecule cm^{-3}, $p_{He} = 1$ bar. The points are amplitudes obtained by the fitting of the experimental temporal profiles (parameter A, see text). The values are normalized to the maximum value at 330 nm. Two experimental curves were fitted at each wavelength, the average of the two measurements is shown. The solid line is the experimental absorption cross section of molecular chlorine[9] normalized to the maximum value.

The parameters of this curve are expressed in terms of the yield (ϕ) of Cl atoms per one photodissociated oxalyl chloride molecule; the absorption cross-sections of oxalyl chloride at the wavelengths 193 nm ($\sigma_{OxCl,\ 193}$), 210 nm ($\sigma_{OxCl,\ 210}$) and λ, ($\sigma_{OxCl,\ \lambda}$), the absorption cross-section of molecular chlorine at the probing wavelength ($\sigma_{Cl2,\ \lambda}$), the concentration of oxalyl chloride, [OxCl], the rate constant of reaction 1, k_1, and the change in the absorbance of oxalyl chloride at the probing wavelength λ and 210 nm (($\{\ln(I/I_0)\}_{OxCl,\lambda}$ and ($\{\ln(I/I_0)\}_{OxCl,210}$) due to its photodissociation (see Appendix). The value of $\{\ln(I/I_0)\}_{OxCl,210}$ was measured independently at the same experimental conditions. The value of $\{\ln(I/I_0)\}_{OxCl,\lambda}$ was calculated using the absorption cross-sections listed in Table 1. Parameter $G = \exp(-\sigma_{OxCl,193}[OxCl]l)$ was calculated using the independently measured absorption cross-section of oxalyl chloride at 193 nm ($\sigma_{OxCl,193}$, Table 1). Parameters A and B were used as fitting parameters. An additional check was performed on the assignment of the observed absorption in the range 270−390 nm to molecular chlorine. In this case, parameter $A = -(\sigma_{Cl2,\lambda}/\sigma_{OxCl,210})\{\ln(I/I_0)\}_{OxCl,210}\phi/2$ is expected to be proportional to the Cl_2 absorption cross-section. The absorption temporal profiles were measured over the spectral range 270−390 nm. The profiles were fitted with expression 2, using A and B as fitting parameters. The parameters A obtained in this way were normalized on the value at $\lambda = 330$ nm. The normalized values of the parameter A correlate well with the absorption spectrum of molecular chlorine. The correlation is shown in Figure 5. Parameter B in expression 2 incorporates the reaction rate constant k_1 for the recombination of chlorine atoms (reaction 1): $B = \sigma_{Cl2,\lambda}/(4\sigma_{OxCl,193}[OxCl]\ k_1[He])$. The absorption temporal profiles were measured at λ =330 nm with the oxalyl chloride concentration varied within the range $1.2 \times 10^{16} - 2.5 \times 10^{16}$ molecule cm^{-3}. The termolecular third-order rate constant of reaction 1 yielded by a linear fit of the data obtained in the coordinates B^{-1} vs. [OxCl] is: $k_1 = (4.50 \pm 0.55) \times 10^{-33}$ cm^6 molecule^{-1} s^{-1}. This value is in agreement within the experimental error with the value $(3.86 \pm 0.54) \times 10^{-33}$ cm^6 molecule^{-1} s^{-1} reported by Hippler and Troe.[8] Thus, both the observed spectrum and the measured value of the rate constant confirm the assignment of the absorption in the range 270−390 nm to the molecular chlorine formed in the recombination of chlorine atoms (reaction 1).

TABLE 2. Photodissociation Yield of Chlorine Atoms, ϕ, in Photodissociation of Oxalyl Chloride at 193.3 nm

p_{He}/bar	ϕ
1	1.88 ± 0.08
10	2.01 ± 0.08
101	1.97 ± 0.12

The parameters A obtained from the fits of the temporal absorption profiles measured at $\lambda = 330$ nm and the changes in the absorption at $\lambda = 210$ nm due to the photodepletion of oxalyl chloride were used to calculate the concentrations of molecular chlorine formed and the concentrations of photodissociated oxalyl chloride. The literature value of the absorption cross-sections of molecular chlorine $\sigma_{Cl2,330} = 2.56 \times 10^{-19}$ cm^2 molecule^{-1} was used.[9] The absorption cross-section of oxalyl chloride used in the calculation, $\sigma_{OxCl,210} = 2.46 \times 10^{-18}$ cm^2 molecule^{-1}, is determined in this work (Table 1). The experiments were performed at three buffer gas (helium) pressures, $p_{He} = 1$, 10, and 101 bar. The absorption cross-section of molecular chlorine at 330 nm was assumed to be independent of the buffer gas pressure over the range 1−101 bar. In the region 270−390 nm, molecular chlorine Cl_2 has broad continuous absorption due to the transition from the ground state to the dissociative state $^1\Pi(1_u)$.[10] The values of the photodissociation yield of chlorine atoms, ϕ, (the number of chlorine atoms per one photodissociated molecule of oxalyl chloride) obtained in this way are presented in Table 2.

An additional check was made for dependence of the quantum yield of the photodissociation of oxalyl chloride on the buffer gas pressure. The quantum yield is proportional to the ratio given in eq 3. This ratio is expected to be pressure independent if the quantum yield is pressure independent

$$\phi_{Cl} \propto \frac{\{\ln (I/I_0)\}OxCl_{210}}{(1 - \exp (-\sigma_{oxCl,193}[OxCl]l))} \qquad (3)$$

In this expression, the denominator, proportional to the absorbed energy of the laser radiation at 193.3 nm, can be calculated. In the experiments with constant laser pulse energy, the measured ratio at $p_{He} = 100$ bar was 0.93 ± 0.08 of the ratio obtained at $p_{He} = 1$ bar. Therefore, within the experimental error, no pressure dependence of the quantum yield of dissociation of oxalyl chloride was observed. It means that no appreciable collisional quenching of oxalyl chloride molecules photoexcited at 193 nm occurs at helium pressures up to 100 bar.

Discussion

The experimental results can be summarized as follows. Photoexcited at 193 nm molecules of oxalyl chloride dissociate so fast that they are not collisionally quenched at helium pressures up to 100 bar. Two (within the experimental error) Cl atoms appear from the photodissociation of oxalyl chloride molecule. These results are in agreement with the mechanism of the oxalyl chloride photodissociation suggested by Suits with co-workers[4,5] based on their experimental study of oxalyl chloride collision-free photodissociation in molecular beam. Ahmed et al.[4] studied photodissociation of oxalyl chloride at 235 nm with an angle- and the translational energy resolved detection of the observed products of photodissociation, CO and Cl. Both fragments were found to have quite similar bimodal translational energy distributions. The fast components (for Cl

atoms about one-half of the total yield) of these distributions for both Cl atoms and CO molecules were anisotropic. This lead the authors to the conclusion that after absorption of one photon, oxalyl chloride molecules dissociate on a time scale shorter than that of the period of rotation, giving rise to three fragments in one step

$$(ClCO)_2 + h\nu \rightarrow CO + Cl + ClCO \quad \Delta H^0_{298} = 368.4 \text{ kJ mol}^{-1} \quad (4)$$

The slow components of CO and Cl were attributed to a secondary, also fast, process of dissociation of excited radical ClCO*, which is formed in reaction 4 with the energy sufficient for dissociation

$$ClCO^* \rightarrow Cl + CO \quad \Delta H^0_{298} = 32.6 \text{ kJ mol}^{-1} \quad (5)$$

The enthalpies of reactions 4 and 5 were calculated using the literature data on the standard enthalpies of formation of the species involved: $\Delta H^0_{f,298}((ClCO)_2) = -335.8 \pm 6.3$ kJ mol^{-1},[11] $\Delta H^0_{f,298}(ClCO) = -21.8 \pm 2.5$ kJ mol^{-1},[12] $\Delta H^0_{f,298}(CO) = -110.53$ kJ mol^{-1} [13] and $\Delta H^0_{f,298}(Cl) = 121.3$ kJ mol^{-1}.[13]

Hemmi and Suits studied photodissociation of oxalyl chloride at 193 nm ($h\nu = 620$ kJ mol^{-1}) and also found similar bimodal translational energy distributions for CO and Cl formed. The measured distribution for chlorine atoms is 51% of Cl atoms in the fast and 41% in the slow component. The conclusion was made that the photodissociation dynamics of oxalyl chloride at 193 nm are similar to that at 235 nm. The fraction of ClCO radicals formed in process 4 with energy sufficient to dissociate via process 4 was estimated at ca. 82%. Therefore, according to the results of these studies, only ca. 9% of Cl atoms contained in the photodissociated OxCl molecules remain bound in the ClCO fragment.

On the basis of the process scheme suggested by Suits et al., the following picture of the photodissociation of oxalyl chloride is expected for the experiments being described in this paper, i.e., in the presence of a buffer gas and collisions:

One chlorine atom is formed immediately in the photodissociation reaction 4. About 82% of the COCl radicals that are produced have enough energy to dissociate. The dissociation of these excited radicals occurs rapidly. The pressure falloff curve of the rate constant of unimolecular dissociation of ClCO radical can be used to estimate the pressure region where the collisional quenching can compete with their dissociation. The position of the falloff region was estimated based on the analogy with other three-atomic species. The "center of the fall-off curve" was based on the approach developed by the CODATA Task Group on Chemical Kinetics.[14] The "center" corresponds to the concentration of the buffer gas molecules $[M]_c$ at which the extrapolated low-pressure limit of the rate constant is equal to its high-pressure limit. The CODATA list provides the values of $[M]_c$ for reactions $F + O_2 + M \rightarrow FO_2 + M$ and $O + O_2 + M \rightarrow O_3 + M$. These reactions are reverse reactions of dissociation of the corresponding three-atomic species. The pressure falloff curves are, of course, the same. The estimated $[M]_c$ values ($M = N_2$) are 2.7×10^{21} molecule cm^{-3} ($T = 300$ K) and 5×10^{21} molecule cm^{-3} ($T = 295$ K), respectively.[14] These concentrations, $[M]_c$, correspond to pressures of about 100−200 bar at room temperature. The position of the falloff center, $[M]_c$, depends on the activation barrier for dissociation. The barrier for ClCO dissociation (24.6 kJ mol^{-1} in the low-pressure limit)[12] is much lower than those for FO_2 (98.9 kJ mol^{-1} in the low-pressure limit)[15] and O_3 (96.2 kJ mol^{-1} in the low-pressure limit).[16] This means that the transition pressure for ClCO should be much higher than for FO_2 and O_3. The transition pressure is mainly determined by the competition of the collisional deactivation and dissociation of the molecules activated to the energy just above the dissociation barrier. The internally excited ClCO radicals produced in the photodissociation of oxalyl chloride might have much higher excitation energy. Due to the fast increase of the dissociation rate with the excess energy, higher pressures are required for the collisional stabilization to compete with the dissociation. Therefore, it could be anticipated that activated ClCO radicals dissociate without any quenching at $p_{He} = 1$ and 10 bar. They were estimated by Hemmi and Suits to be about 82% of the total ClCO arising in reaction 4. Partial quenching could be expected at $p_{He} = 100$ bar. ClCO radicals, which are produced with insufficient energy to dissociate as well as the radicals stabilized below the dissociation level in collisions then undergo the usual thermal dissociation via the collisional activation by the buffer gas (reaction 5). The fraction of ClCO radicals with insufficient energy for dissociation is estimated by Hemmi and Suits about 18% of the total ClCO produced in reaction 4. The lifetime of the thermalized ClCO radicals with respect to reaction 4 was estimated based on the rate constant measured by Nicovitch et al.:[12] $\tau = 2$ μs at p=1 bar, $\tau = 0.2$ μs at p =10 bar and $\tau = 0.02$ μs at $p = 100$ bar, respectively, with nitrogen as a buffer gas. These estimates are not anticipated to be much different for helium as a buffer gas where lower efficiency of collisions is compensated by higher collision frequency.

In the kinetic experiments at pressures below 1 bar, care should be taken to perform the measurements on the time scale sufficiently longer than the time required for the dissociation of ClCO radicals. The lifetime is proportional to the inverse bath gas pressure. At pressures of ca. 0.01 bar, the anticipated lifetime at ambient temperature is 0.2 ms. Therefore, kinetic measurements free of ClCO radical interference are possible in the millisecond time domain. At elevated temperatures, ClCO radical dissociation rate is less restrictive, due to the faster dissociation. The apparent activation energy for dissociation of ClCO is 24.6 kJ mol^{-1}.[12] At 600 K, the dissociation of ClCO radical is 140 times faster and takes only 1.5 μs at 0.01 bar bath gas pressure, which allows measurements in the microsecond time domain.

Initial concentrations of Cl atoms in this work were ca. $(1-2) \times 10^{15}$ molecule cm^{-3}. The reaction of ClCO radicals with chlorine atoms (reaction 6) can possibly compete with the reaction of unimolecular dissociation only at $p_{He} = 1$ bar and only if the rate constant of this reaction is ca. 10^{-10} cm^3 molecule^{-1} s^{-1} (the true rate constant is unknown).

$$ClCO + Cl \rightarrow Cl_2 + CO \quad (6)$$

It should be pointed out that reaction 6 leads to a "prompt" formation of molecular chlorine. However, the experiments in this work are not capable of discriminating the molecular chlorine formation via reaction 6 and via the recombination reaction 1 if the relative contribution of chlorine molecules formed in reaction 6 is small (<15%). At higher pressures ($p_{He} = 10$ and 101 bar) reaction 6 can be neglected.

Reaction of chlorine atoms with the precursor molecule, oxalyl chloride (reaction 7), is expected to be very slow in view of the weak Cl−Cl bond in molecular chlorine and relatively strong Cl−C bond in oxalyl chloride. The chlorine abstraction routes are

$$Cl + (COCl)_2 \rightarrow Cl_2 + CO(COCl) \quad (7a)$$

$$\rightarrow Cl_2 + CO + COCl \quad (7b)$$

The actual rate constant of this reaction is not known. In the current experiments, this reaction would lead to the acceleration of the molecular chlorine formation and distortion of the second-order kinetics (Figure 4). A conservative estimate derived based on the kinetic curve in Figure 4 gives $k_7 < 4 \times 10^{-14}$ $cm^3molecule^{-1}s^{-1}$. Channel 7b is endothermic by 82 kJ mol^{-1}. Channel 7a is also expected to be endothermic, based on the typical weak bond energies in RCO radicals. In addition, all known reactions of free radicals with phosgene are quite slow.[17]

In conclusion, the mechanism of oxalyl chloride dissociation suggested by Suits and coauthors based on a collision-free molecular beam experiments is in agreement with the results of the experiments in a bath-gas environment described in this work. According to the results of Suits et al. and the analysis above, under 193 nm light photodissociation of oxalyl chloride produces chlorine atoms and internally excited ClCO radicals. The photodissociation process is not quenched to any appreciable degree at pressures up to 100 bar. The majority of the residual chlorine atoms that originate from the internally excited ClCO radicals (ca. 91%) appear promptly on the time-scale shorter than the time between collisions even at elevated pressures. The rest of the chlorine atoms that originate from the ClCO radicals do not have sufficient initial energy for dissociation (about 9%) appears on a longer time-scale (ca. 2 μs at 1 bar and at shorter times at elevated pressures) via thermal dissociation of ClCO radical.

Production of phosgene, $COCl_2$, observed in the photodissociation of oxalyl chloride in solid Xe matrix by Shroeder et al.,[3] can be attributed to the "cage" effect of solid matrix resulting in recombination Cl and ClCO formed in reaction 4.

Conclusions

Under proper conditions, photodissociation of oxalyl chloride at 193 nm represents a clean source of chlorine atoms. The photodissociation yield of the process is two chlorine atoms per dissociated oxalyl chloride molecule within the experimental error. The process leads to the production of chlorine atoms and relatively inert carbon monoxide. This, together with the relatively large absorption cross-section of oxalyl chloride in the UV region make oxalyl chloride a prospective candidate for a "clean" photolytic source of chlorine atoms for kinetic studies.

It should be mentioned, however, that the current results could not be automatically transferred to other wavelengths of photolysis. The dissociation yields and lifetimes can depend strongly on the energy deposition. Although oxalyl chloride shows appreciable absorption at 248 nm and other excimer laser lines (Figure 1), further study is required to access the precursor quality and the chlorine atom yields at these wavelengths.

Appendix

An analytical expression for the absorption of molecular chlorine formed in the reaction of chlorine atom recombination under the conditions of a nonuniform axial distribution due to an arbitrary degree of absorption of the photolytic light is derived below. The expression is for the temporal profile of the absorption (base e, $Abs(t) = -\ln(I/I_0)_{Cl2,\lambda}$) of molecular chlorine Cl_2, which is formed in the recombination of chlorine atoms (reaction 1). Chlorine atoms are formed in the photodissociation of oxalyl chloride (hereafter referred to as OxCl). The photolytic light intensity I_{193} decreases exponentially along the cell axis: $I_{193}=I_{193,0}\exp(-\sigma_{OxCl,193}[OxCl]x)$, where x is the coordinate along the cell axis, $x = 0$ at the beginning and $x = l$ at the end of the cell, [OxCl] is the number density of the precursor molecules. The initial concentration ($t = 0$) of Cl atoms produced from OxCl is x-dependent

$$[Cl]_{x,0} = [Cl]_{0,0} \exp(-\sigma_{OxCl,193}\,[OxCl]\,x) \quad (A1)$$

The initial concentration of Cl atoms can be derived from the known photodepletion of oxalyl chloride concentration $\Delta[OxCl]_x$

$$[Cl]_{x,0} = -\phi\Delta[OxCl]_x \quad (A2)$$

where ϕ is the number of Cl atoms produced per one photodissociated OxCl molecule. The value $\Delta[OxCl]_x$ determines the absorption photodepletion of OxCl at 210 nm, $\{\ln(I/I_0)\}_{OxCl,210}$, which is measured in an independent experiment

$$\{\ln (I/I_0)\}_{OxCl,210} = -\sigma_{OxCl,210}\int_0^l \Delta[OxCl]_x dx \quad (A3)$$

Substitution of eqs A1 and A2 into eq A3 and integration over x gives the initial concentration at the reactor entrance, $[Cl]_{0,0}$

$$[Cl]_{0,0} = \frac{\phi\{\ln (I/I_0)\}_{OxCl,210}\sigma_{OxCl,193}[OxCl]}{\sigma_{OxCl,210}(1 - \exp(-\sigma_{OxCl,193}[OxCl]l))} \quad (A4)$$

The time-dependence of the concentration of chlorine atoms disappearing in reaction 2 is given by eq A5

$$[Cl]_{x,t} = \frac{[Cl]_{x,0}}{1 + 2k_1[He][Cl]_{x,0}(t - t_0)} \quad (A5)$$

where t_0 is the time of the laser pulse. The characteristic time of chlorine atom production (<2 μs) is assumed to be much shorter than the characteristic time of chlorine atom recombination (ca. 2 ms). Only recombination reaction 1 is assumed to be responsible for the disappearance of chlorine atoms. The material balance relation

$$[Cl_2]_{x,t} = \frac{[Cl]_{x,0} - [Cl]_{x,t}}{2} \quad (A6)$$

The instant spatial distribution of molecular chlorine

$$[Cl_2]_{x,t} = [Cl]_{x,0}\frac{k_1[He][Cl]_{x,0}(t - t_0)}{1 + 2k_1[He][Cl]_{x,0}(t - t_0)} \quad (A7)$$

Integrating the instantaneous spatial profile of molecular chlorine A7 along the reactor axis and using A4−A6, obtain

$$-\{\ln (I/I_0)\}_{Cl2,\lambda} = \sigma_{Cl2,\lambda} l\int_0^l [Cl_2]_{x,t}dx = \frac{\sigma_{Cl2,\lambda}}{\sigma_{OxCl,193}[OxCl]4k_1[He](t - t_0)} \times \left\{2k_1[He](t - t_0)([Cl]_{0,0} - [Cl]_{l,0}) - \ln\left(\frac{1 + 2k_1[He][Cl]_{0,0}(t - t_0)}{1 + 2k_1[He][Cl]_{l,0}(t - t_0)}\right)\right\} \quad (A8)$$

Three dimensionless combinations A, B, and G are introduced

$$A = \frac{1}{2}\phi\frac{\sigma_{Cl2,\lambda}}{\sigma_{OxCl,210}}\{\ln (I/I_0)\}_{OxCl,210} \quad (A9)$$

$$B = \frac{\sigma_{Cl2,\lambda}}{4\sigma_{OxCl,193}[OxCl]k_1[He]} \quad (A10)$$

$$G = \exp (-\sigma_{OxCl,193}[OxCl]l) \quad (A11)$$

Equation 8 becomes

$$-\{\ln (I/I_0)\}_{Cl2,\lambda} = A - \frac{B}{(t-t_0)}\ln\left\{\frac{\left[1+\frac{A(t-t_0)}{B(1-G)}\right]}{\left[1+\frac{AG(t-t_0)}{B(1-G)}\right]}\right\} \quad (A12)$$

Finally, taking into account the impact of the photodepletion of oxalyl chloride at the probing wavelength λ, $C = \{\ln(I/I_0)\}_{OxCl,\lambda}$, obtain

$$\mathrm{Abs}(t) = -\ln (I/I_0)_\lambda = A - C - \frac{B}{(t-t_0)}\ln\left\{\frac{\left[1+\frac{A(t-t_0)}{B(1-G)}\right]}{\left[1+\frac{AG(t-t_0)}{B(1-G)}\right]}\right\} \quad (A13)$$

This function was used to fit the experimental absorption temporal profiles.

Acknowledgment. This work was supported by the Petroleum Research Fund administered by the American Chemical Society (Grant # 31640-AC6).

References and Notes

(1) Krasnoperov, L. N.; Chesnokov, E. N.; Panfilov, V. N. *Chem. Phys.* **1984**, *89*, 297.

(2) Jasinski, J. M.; Becerra, R.; Walsh, R. *Chem. Rev.* **1995**, *95*, 1203.

(3) Schroeder, W.; Monnier, M.; Davidovics, G.; Allouche, A.; Verlaque, P.; Pourcin, J.; Bodot, H. *J. Mol. Struct.* **1997**, *197*, 227.

(4) Ahmed, M.; Blunt, D.; Chen, D.; Suits, A. *J. Chem. Phys*. **1997**, *106*, 7617.

(5) Hemmi, N.; Suits, A. G. *J. Phys. Chem. A* **1997**, *101*, 6633.

(6) Krasnoperov, L. N.; Mehta, K. *J. Phys. Chem. A* **1999**, *103*, 8008.

(7) International Thermodynamic Tables of the Fluid State. Helium-4. *IUPAC Division of Physical Chemistry Commission on Thermodynamics and Thermochemistry Thermodynamics Tables Project*; Angus, S., de Reuck, K. M., McCarty, R. D., Eds; Pergamon Press: New York, 1977.

(8) Hippler, H.; Troe, J.*Chem. Phys. Lett.* **1973**, *19*, 607.

(9) DeMore, W. B.; Sander, S. P.; Golden, D. M.; Hampson, R. F.; Kurylo, M. J.; Howard, C. J.; Ravishankara, A. R.; Colb, C. E.; Molina, M. J. *Chemical Kinetics and Photochemical Data for Use in Stratospheric Modeling, JPL Publication 92−20*, Jet Propulsion Laboratory: Pasadena, 1992; p 122.

(10) Okabe, H. *Photochemistry of Small Molecules*; Wiley: New York, 1978.

(11) Walker, L. C.; Prophet, H. *Trans. Faraday Soc*. **1967**, *63*, 879.

(12) Nicovitch, J. M.; Kreutter, K. D.; Wine, P. H. *J. Chem. Phys*. **1990**, *92*, 3539.

(13) Atkinson, R.; Baulch, D. L.; Cox, R. A.; Hampson, R. F., Jr.; Kerr, J. A.; Troe, J. *J. Phys. Chem. Ref. Data* **1989**, *18*, 881.

(14) Baulch, D. L.; Cox, R. A.; Hampson, R. F., Jr.; Kerr, J. A.; Troe, J., and Watson R. T. *J. Phys. Chem. Ref. Data* **1980**, *9*, 295.

(15) Atkinson, R.; Baulch, D. L.; Cox, R. A.; Hampson, R. F., Jr.; Kerr, J. A.; Rossi, M. J.; Troe, J. *J. Phys. Chem. Ref. Data* **1997**, *26*, 521.

(16) Lunin, B. S.; Kuricheva, O. V.; Zhitnev, Yu. N. *Russ. J. Phys. Chem. (Engl. Transl.)* **1986**, *60*, 1229.

(17) Westley, F.; Herron, J.; Frizzell, D.; Hamson, R.; Mallard, G.; Mirokhin, Y.; Blackslee, D. M. *The NIST Chemical Kinetics Database. NIST Standard Reference Database 17−2Q98*; 1998, National Institute of Standard and Technology: Gaithersburg, MD 20899.